A molecular dynamics study and the electronic properties of amorphous carbon using the Tersoff potential

1993 J. Phys.: Condens. Matter 5 9157

(http://iopscience.iop.org/0953-8984/5/49/018)

J. Phys.: Condens. Matter 5 (1993) 9157–9168. Printed in the UK

A molecular dynamics study and the electronic properties of amorphous carbon using the Tersoff potential

U Stephan and M Haase

Department of Physics, Technical University of Chemnitz–Zwickau, D-09009 Chemnitz, PSF 964, Federal Republic of Germany

Received 21 July 1993, in final form 1 October 1993

Abstract. To obtain qualitatively different amorphous carbon networks we carried out molecular dynamics simulations at different mean atomic densities using the Tersoff potential. Differences among the radial distribution functions obtained as well as among the ratio of threefold- and fourfold-coordinated atoms according to the mean densities are discussed. The electronic stability of the models is investigated by means of their total densities of states which are characterized by significant defect bands. These bands are ascribed to the uncorrelated free-atomic p orbitals occurring in the models. The effect may be quantified by a simple π bonding analysis which estimates the relative number of non-bonding and of bonding and antibonding π states by calculating the number of unbonded hybrid orbitals and topological π defects. For a justification, a number of local densities of states are calculated.

1. Introduction

Interest in computer-assisted modelling of covalent amorphous structures has been growing for many years. The unique structural characterization of amorphous carbon (a-C) films remains, however, a very difficult problem due to the variety of possible chemical bonding in the atomic network. The carbon atoms in the a-C films may be arranged within a twofold, threefold or fourfold coordination. As a result, the bond lengths and bond angles may show a wide variation and hence cause qualitatively different structures. The structure formation depends on several conditions: the deposition method, the temperature of the process, the initial substances (graphite, benzene, methane and so on) and the substrate material. As is well known, the resulting a-C films are classified either as hard, dense and diamond-like films, or as softer and graphite-like films [1, 2]. The hard films, which are prepared by arc evaporation techniques, have been assumed to be mostly composed of fourfold-coordinated atoms, with a fraction of such sp^3 hybridized atoms of approximately 0.9 [3–6]. These films are therefore also known as tetrahedrally bonded amorphous carbon (ta-C) or amorphous diamond (a-D). The mass densities ρ of these films range from about $2.5\,g\,cm^{-3}$ up to $3.0\,g\,cm^{-3}$. On the other hand, the less dense a-C films prepared by RF sputtering are shown to contain more than 90% threefold-coordinated atoms, giving rise to mass densities less than approximately $2.4\,g\,cm^{-3}$. These films are probably not composed of ordered hexagonal ring structures, but exhibit distorted threefold environments [7, 8]. Additionally, structures that contain only little hydrogen ($\leqslant 4\%$) but a nearly equal number of sp^3 and sp^2 sites may also exist [2, 9].

In general, the experimental determination of the structure using scattering methods is difficult, because the resulting radial distribution function is not unambiguously related to the spatial arrangement of the carbon atoms. Further, the experimentally obtained mass

0953-8984/93/499157+12$07.50

densities as well as sp^3/sp^2 fractions must be regarded with some caution because of uncertainties up to about 25%. Being aware of these problems, we want to show in this paper how the structure of a carbon network varies with a change in the mean density of the network. We generated our models via a molecular dynamics simulation using the empirical interatomic potential of Tersoff [10] in the microcanonical ensemble with periodic boundary conditions (see section 2). This potential was chosen because of its general form, which is dependent on the actual local environment of a given atom. The generation of a carbon network including twofold-, threefold- and fourfold-coordinated atoms may thus be enabled. Nevertheless, the number of parameters is not too large to be adjusted in a straightforward fashion. At this stage, however, the role of hydrogen in the structure formation can only be discussed qualitatively. To obtain information about the stability of the generated networks, in section 3 we examine their electronic structure by calculation of total and local densities of states. This may prove to be a useful extension to the common discussion in this field, where conclusions about the quality of the generated networks using this potential are based only upon their mechanical and structural properties. Finally, we provide conclusions from the present work in the final section.

2. Structure generation

A molecular dynamics simulation with periodic boundary conditions allows one to fix the mean density of the system exactly. We present data for our three analysed structures with densities of 2.00, 2.50 and 3.00 $g\,cm^{-3}$ containing an equal number of atoms (512). This ensures a good basis for a statistical comparison of the three models. The key problem in performing a molecular dynamics simulation is to choose a correct interatomic potential. There are a number of different empirical potentials in the literature, most of which have been devised for the case of silicon (for a recent review see Cook and Clancy [11]). The potential we require for carbon should take into consideration the covalent bonding nature of the carbon atoms, the resulting different bond lengths and bond angles, and the role of the π electrons. The potential derived by Tersoff counts the number of neighbours of a given atom and, in this way, controls the bond lengths and bond angles. An explicit π-bonding term, however, is missing in this potential. The influence of the π electrons on the bonding energy is therefore considered independently of the actual types and arrangements of neighbours on a level of graphite-like atoms only. There have been a few attempts with Tersoff-like potentials to take into account the formation of π bonds in the network [12, 13], but the analytical expressions for these potentials are rather complicated. Furthermore, these potential concepts cannot avoid a large number of parameters (> 20) which makes the correct adjustment for different structures a tricky problem. Therefore, we still apply the original potential with the hope of gaining some insight about the drawbacks of this method as well as some possible improvements. The potential used is the same as that given in [10]:

$$V_{ij} = f_c(r_{ij})[A\exp(-\alpha_1 r_{ij}) - Bb_{ij}\exp(-\alpha_2 r_{ij})] \tag{1}$$

$$b_{ij} = (1 + \beta^n \xi_{ij}^n)^{-1/2n} \tag{2}$$

$$\xi_{ij} = \sum_{k \neq i,j} f_c(r_{ik}) g(\theta_{ijk}) \tag{3}$$

$$g(\theta) = 1 + (c/d)^2 - c^2/[d^2 + (h - \cos\theta)^2]. \tag{4}$$

Here i, j and k label the atoms of the system, r_{ij} is the bond length between the atoms i and j and θ_{ijk} is the bond angle between bonds ij and ik. The function $f_c(r)$ represents

the cutoff function limiting the range of the potential. The sum in (3) counts for $g = 1$ the neighbours of atom i except atom j. The potential has the characteristic form of a Morse potential, but three-body effects are additionally included in b_{ij}. It is important to know that the given parameter set for carbon in [10] correctly reproduces the bond length for a fourfold coordinated atom (as in diamond: 1.54 Å), while the bond length for a threefold coordinated atom is 1.46 Å instead of 1.42 Å as in graphite. Consequently, the resulting mean bond length between two threefold-coordinated atoms may be somewhat too high, and the first peak position in the radial distribution function is shifted to higher values.

We start our molecular dynamics simulation with a randomized spatial atomic configuration at a temperature of about 5000 K. During the thermalization the system is cooled down to a temperature of 300 K. In the following equilibration run (10^{-13} s) the information for a time- and configurationally-averaged reduced radial distribution function (RRDF) is obtained.

Statistical data for the three generated models are listed in table 1. Choosing the densities as mentioned above we obtain networks in which most of the atoms are threefold coordinated. This portion decreases with increasing density, but it still predominates at the relatively high density of 3.00 g cm^{-3}. The Monte Carlo simulations by Kelires [14] using the same potential show analogous results for structures generated under low pressure (e-C). This fact is clear, since our molecular dynamics procedure in the NVE ensemble works with zero pressure. The relaxed structures are stable with respect to the potential used, but the question is whether or not these structures are realistic. In section 3, therefore, we investigate the electronic structure (DOS) of the generated amorphous networks. It will be seen from this point of view that a further relaxation including the electronic structure may change the character of the network.

Table 1. Statistical data of the models and of graphite (gr) and diamond (di). The density is measured in g cm^{-3}. r_1 and r_2 denote the position of the first and second peak in the RRDF; $\bar{z}$ denotes the mean coordination number; C4, C3 and C2 represent the content of atoms with $z = 4$, $z = 3$ and $z = 2$ (in %); $\bar{\theta}$, $\Delta\theta$ are the related mean bond angle and standard deviation (in degrees).

							C2		C3		C4	
Density	r_1 (Å)	r_2 (Å)	$\bar{z}$	C2	C3	C4	$\bar{\theta}$	$\Delta\theta$	$\bar{\theta}$	$\Delta\theta$	$\bar{\theta}$	$\Delta\theta$
2.00	1.50	2.61	2.93	13	80	7	126.5	5.4	118.9	5.5	109.2	10.8
2.50	1.49	2.55	3.05	5	79	16	123.6	3.1	118.6	5.9	109.3	9.7
3.00	1.51	2.55	3.33	1	66	34	123.8	2.5	118.6	5.5	109.2	8.9
2.26 (gr)	1.42	2.46	3.00	0	100	0	—	—	120	—	—	—
3.53 (di)	1.54	2.52	4.00	0	0	100	—	—	—	—	109.4	—

The positions of the first peak in the RRDF are in satisfactory agreement with experimental data, but this fact must be regarded with some caution. This position is the result of superimposing the bond length distributions of several types of bonds. Hence, the relative occurrence of different bond types in the network and their lengths are not unambiguously related to the first peak position.

The mean bond angles reproduce well the values required by the potential. At the threefold-coordinated atoms they are only about 1° less than the 120° value needed for a plane neighbour arrangement. The mean bond angles at the fourfold-coordinated atoms agree very well with the diamond angle. Additionally, the variations of the bond angles do not exceed a value of 11°. These facts may serve as a justification for the indirect three-body term that is included in the empirical potential used.

Figures 1 and 2 show the time- and configurationally-averaged reduced radial distribution functions $\gamma(r) = 4\pi r\rho[g(r) - 1]$ of the amorphous structures, and of diamond and graphite, respectively. The resulting RRDF have no double peak around 2.70 Å, as found in the RRDF of diamond. With increasing density the ratio of the amplitudes of the first to the second peak decreases, which is consistent with the increasing number of first neighbours. A striking feature of the curve for the structure with $\rho = 3.00\,\mathrm{g\,cm^{-3}}$ is the small shoulder at 3.00 Å. Results by Gaskell and co-workers [5] for a-C films ($\rho = 3.07\,\mathrm{g\,cm^{-3}}$) exhibit the same feature. In [7] Li and Lannin argued that the absence of this small peak around 3.00 Å implies the absence of a significant fraction of ordered six-membered rings. A detailed analysis of our RRDF in the region between 3.00–3.40 Å shows that the peak (or shoulder) arises from an equipartition of the dihedral angle. Consequently, the distribution of the third-neighbour distance is smeared out and has a plateau in this region. The superposition of this plateau with the tails of the distributions of second neighbours as well as higher-order neighbours gives rise to this peak [15]. The equipartition of the dihedral angle is due to the neglect of the π bonds which favour dihedral angles of 0° and 180° in graphite. Hence in our structures this feature is caused by a random distribution of the atoms in non-planar arrangements.

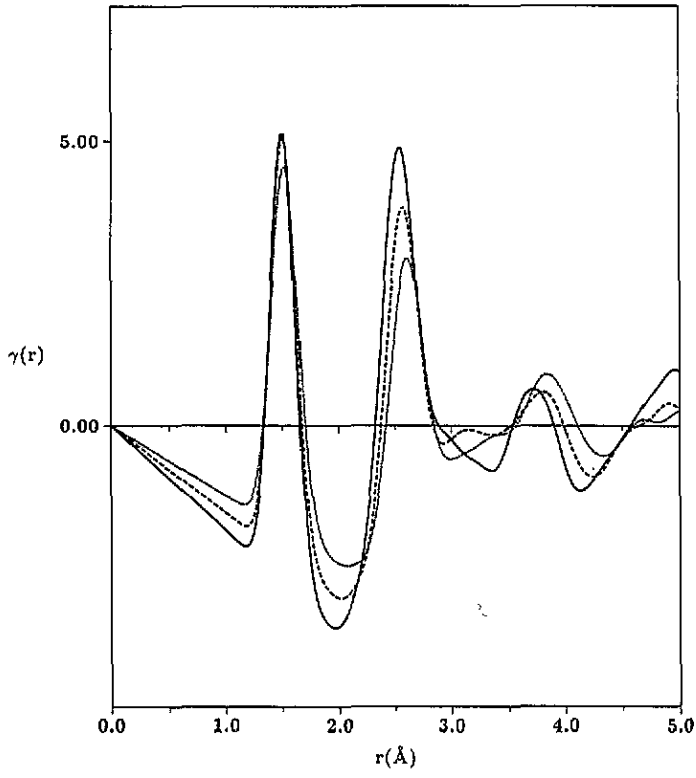

Figure 1. Calculated reduced radial distribution function (RRDF) of the three amorphous C networks. Full curve: $\rho = 3.0\,\mathrm{g\,cm^{-3}}$; broken curve: $\rho = 2.5\,\mathrm{g\,cm^{-3}}$; dotted curve: $\rho = 2.0\,\mathrm{g\,cm^{-3}}$.

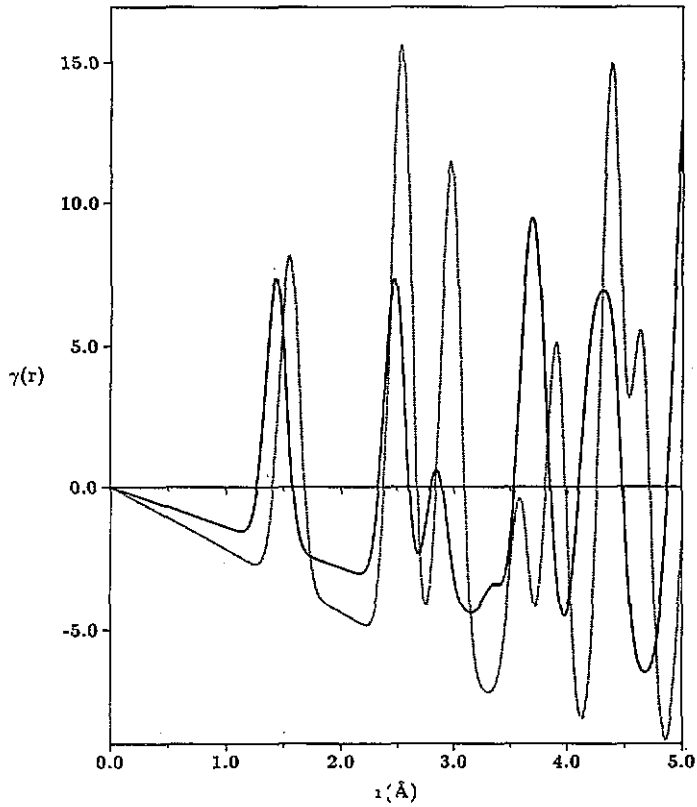

Figure 2. Calculated reduced radial distribution function of diamond (dotted curve) and graphite (full curve).

The scattering-intensity function $F(Q)$ is shown in figure 3. These data are obtained by a Fourier transformation of $\gamma(r)$:

$$F(Q) = \int_0^\infty \gamma(r) \sin(rQ)\, dr. \tag{5}$$

Because of our relatively large unit cell, termination errors in the Fourier transformation are small. The experimental curves of Li and Lannin [7] for a-C with a density of about $2.00\,g\,cm^{-3}$ are in good agreement with our results at the same density. An interesting feature is the double-peak structure near $Q = 10\,Å^{-1}$. According to our results the left peak is lower than the right one, but with increasing mean coordination number the ratio of the peak heights tends to unity. An analysis of the Fourier transformation shows this ratio to be mainly influenced by the first and second correlation spheres, i.e. by the content of threefold- and fourfold-coordinated atoms. A comparison with other experimental and theoretical results [7, 5, 14, 16] leads us to the conclusion that for equal numbers of threefold- and fourfold-coordinated atoms the left peak becomes higher than the right one.

In [14] a so-called 'glass-transition temperature' for the potential of about 2600 K is reported. In figure 4, we show the dependence of the bonding energy on the temperature during a thermalization run. As the initial configuration a network at 300 K, which represents a metastable 'frozen' state, was used. It is obvious that up to a temperature of about

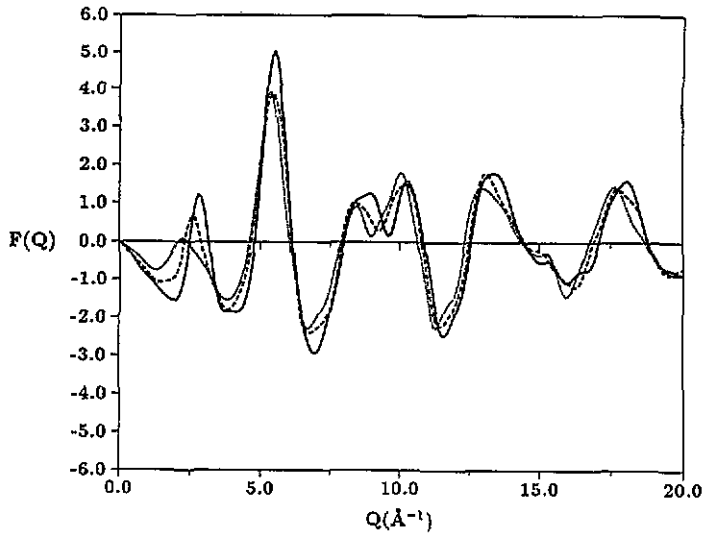

Figure 3. Calculated intensity function $F(Q)$ of the three amorphous networks. The curve form corresponds to figure 1.

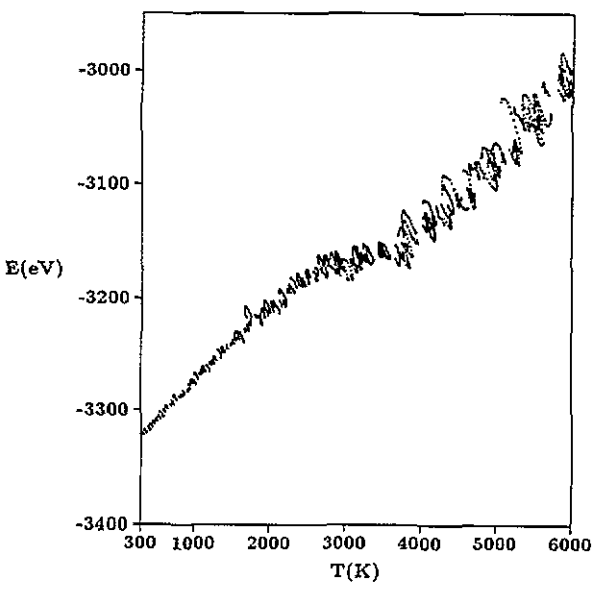

Figure 4. Bonding energy E against temperature T during a thermalization run. At $T = 2600$ K the metastable state was broken and the system relaxed into a new configuration. The energy gain amounts to about 150 eV for 512 atoms after cooling down the system to 300 K.

2600 K the system behaves like a system of harmonic oscillators ($E \sim T$), while above this temperature the slope of the curve is determined by processes which are connected with atomic site interchanges. At about 4300 K this process is terminated. Upon cooling from 6000 K to 300 K, the bonding energy of the system is equal to the value that has been reached by extrapolating the upper part of the curve to $T = 300$ K.

3. Electronic properties

After investigating the structural properties of our computationally obtained systems, we are interested in determining some important electronic features of these systems. For this reason, we have calculated the total electronic density of states (TDOS) of the structures as well as some local densities of states (LDOS) at representative atoms. These calculations were performed by means of the Haydock recursion method [17] with use of an *ab initio* LCAO Hamiltonian and overlap parameters based on a minimal basis of atomic-like orbitals [16]. Within this method, the LDOS projected on some chosen atomic orbital $|\varphi_\mu\rangle$

$$n_\mu(E) = \sum_i |\langle\varphi_\mu|\psi_i\rangle|^2\delta(E-\varepsilon_i) = -\frac{1}{\pi}\,\mathrm{Im}\langle\varphi_\mu|(E-\hat{H})^{-1}|\varphi_\mu\rangle \tag{6}$$

(the sum over all eigenstates $|\psi_i\rangle$ with eigenvalues ε_i), is derived by setting the starting orbital of the recursion equal to $|\varphi_\mu\rangle$. Proceeding with the recurrence equations

$$|u_{-1}\rangle = 0$$
$$b_{i+1}|u_{i+1}\rangle = (\hat{H}-a_i)|u_i\rangle - b_i|u_{i-1}\rangle \qquad i \geqslant 0$$

the given basis set of all atoms will be transformed into a new set $|u_i\rangle$ of orthonormal but successively more remote orbitals related to the atom in question. The Hamiltonian for this basis becomes tridiagonal with matrix elements $a_i = \langle u_i|\hat{H}|u_i\rangle$ and $b_i = \langle u_{i-1}|\hat{H}|u_i\rangle$. The evaluation of the inverse matrix element in (6) results in a continued fraction which may be properly truncated or terminated to reduce numerical effort. For a sufficiently accurate DOS picture we applied the Gaussian quadrature approach [18] using 30 or 50 recursion levels for the TDOS and LDOS calculations, respectively.

The usage of periodic boundary conditions for extending the structures to infinity was taken into consideration by expanding the recursion orbitals into Bloch states. Therefore, the calculation of the new matrix elements a_i, b_i requires an integration over the Brillouin zone of the structures which was approximated by a special-k-point procedure [19, 20] with 216 k vectors. The TDOS is obtained by averaging various recursion runs using initial vectors with randomly weighted orbitals taken from all atoms [21]. For the large number of atoms in our systems, ten recursion runs proved to be sufficient. The correct summation of the so-obtained LDOS is ensured by a Löwdin orthonormalization of the basic atomic orbitals.

First, let us discuss the TDOS of the calculated structures as plotted in figure 5. All structures are characterized by similar densities of states, which can clearly be partitioned into a low-energy σ-like band built from s and p atomic states, and a distinct defect-like band around the Fermi energy that essentially exhibits p-like character. Both bands are separated by a sharp minimum in the TDOS at about $-10\,\mathrm{eV}$. Below this energy the TDOS mainly reflects the bond formation between nearest-neighbour atoms keeping in mind that only σ bonds are favoured within the Tersoff potential used. The defect part, however, stems from the interaction of the remaining atomic states that are not chemically saturated. As may be seen from table 2, the number of eigenstates within this band (the defect-DOS integral, taken between the minima enclosing this DOS part) strongly correlates with the number of atomic hybrids that do not contribute to σ bonds (non-σ-bonded orbitals). Because a π-like interaction term is missing in the potential, the atoms do not tend to form π bonds through any physical reason. As a consequence, the shape of this band is more reminiscent of the Gaussian-like defect band normally assumed in tetrahedrally bonded semiconductors such as a-Si (see, for example, [22]) than of the double-peak structure found in a-C:H models

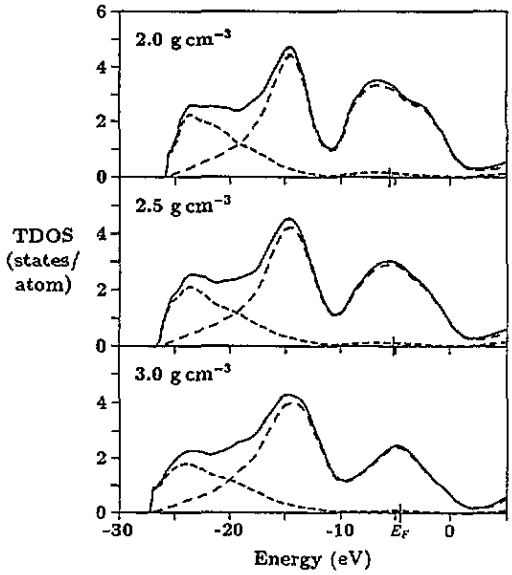

Figure 5. Total densities of states of the calculated structures (full curves). Short-dash curves: s partial TDOS; long-dash curves: p partial TDOS.

Table 2. Number and classification of all non-σ-bonded orbitals, and weight of the defect-part of the calculated TDOS (all values related to one atom).

Density ($g\,cm^{-3}$)	Non-σ-bonded orbitals			Defect-DOS integral
	sp^x hybrids	p orbitals	Sum	
2.00	0.199	0.867	1.066	1.076
2.50	0.141	0.750	0.891	0.886
3.00	0.076	0.596	0.672	0.638

via an *ab initio* LCAO–MD relaxation [23]. Furthermore, the width of this band cannot grow to such an extent that a remarkable overlap with the σ band emerges.

To gain a deeper understanding of these defect bands, we have investigated the π bonding character of our structures in a more quantitative manner. To this end, we applied the following simplified model which was deduced after comparing several LCAO calculations on small hydrocarbon clusters [24, 25]. As a first step, we classify the free orbitals of threefold- and twofold-coordinated atoms with respect to their p characters; if this p portion is larger than a certain value these orbitals are referred to as p-like, otherwise as sp^x (see table 2). (We used a value of 93%, which is also suitable to distinguish between sp- and sp^2-like twofold-coordinated atoms, where only the latter occur in Tersoff-relaxed structures.) Both classes of orbitals are treated equivalently, but we bear in mind that the free sp^x hybrids in general produce eigenstates which have somewhat lower energy compared with the p-like ones. Continuing, two under-coordinated atoms may be considered as π-like bonded if the overlap integral of their free hybrids exceeds another critical value necessary to create a significant minimum in the LDOS at an isolated pair of sp^2 atoms (0.042 chosen for our LCAO parameters). In particular, the case of twofold-coordinated atoms is treated by free orbitals that ensure the maximum possible overlap to the neighbouring atoms. Now we have estimated the number of randomly created bonding and non-bonding π states of the

structures (see table 3). First, the latter term is considered to include all unbonded atomic orbitals, i.e. orbitals that do not contribute to any σ or π bond. We then performed an analysis of the nearest-neighbour bonding matrices of all π-bonded atom groups including more than two atoms. The procedure corresponds to a simple Hückel theory which gives for the eigenvalue $E = 0$ all non-bonding eigenstates. These states may be referred to as topological π defects which for example occur in all odd-membered and some even-membered alternating π clusters. A coarse estimate for the shape of the TDOS near E_F may now be inferred from the ratio of the non-bonding to the bonding and antibonding states: whereas the total weight of the defect bands decreases with increasing density, this π-states ratio increases in the same way. As a result, the defect part of the TDOS becomes smaller for the high-density structures, but its shape varies from being more rectangular-like to becoming similar to an acute angle (see figure 5). Additionally, the relative number of free sp^x hybrids emerging from threefold-coordinated non-sp^2-like atoms and twofold-coordinated non-sp-like atoms decreases (see tables 2 and 3) leading to a reduction of asymmetric parts in the defect TDOS.

Table 3. The number and classification of all unbonded orbitals, and the number of different kinds of π states resulting from all π-like bonded orbitals (all values are related to one atom; bond: bonding, antibd: antibonding).

Density ($g\,cm^{-3}$)	Unbonded orbitals			Non-bonding π	Bond+antibd π	Non-bonding/ bond+antibd
	sp^x hybrids	p orbitals	Sum			
2.00	0.059	0.152	0.211	0.305	0.761	0.40
2.50	0.039	0.162	0.201	0.281	0.610	0.46
3.00	0.033	0.174	0.207	0.268	0.404	0.66

This discussion may be illustrated by local densities of states at various selected atoms. Some typical results are shown in figures 6 and 7. The two structures with the lower mass densities contain about 10% atoms that are only bonded to two nearest neighbours. These atoms exhibit sp^2-like hybridization because a bond angle of about 180° related to sp hybrids is not favoured by the Tersoff potential. Consequently, the LDOS in the defect region (figure 6(*a*)) is first characterized by the atomic p orbital perpendicular to the plane of the atom in question and its two neighbours. Without significant π interaction, this orbital leads to a sharp peak at E_F which is accompanied on the low-energy side by eigenstates that have a significant weight on the free hybrid within the aforementioned plane. The occurrence of a remarkable number of such highly unsaturated atoms, therefore, gives a strong contribution to a TDOS maximum at E_F.

A similar picture is obtained for atoms that possess three nearest neighbours. The parameters entering the Tersoff potential are adjusted in such a way that these atoms tend to form sp^2 bonding arrangements. This leads to about 120° bond angles to the neighbouring atoms which lie, together with the central atom, nearly in one atomic plane. It can be seen that the LDOS of such atoms show a great variety depending on the interactions of the unsaturated orbital to neighbouring atoms. In figure 7(*a*), the LDOS is calculated at a nearly ideal sp^2 hybridized atom that only slightly interacts with neighbouring free p orbitals (maximum overlap 0.023). The non-bonded orbital produces the sharp p peak near E_F. Figure 7(*b*) shows an atom within a configuration being a little bit below our limiting case of 0.042 overlap. The stronger interaction gives rise to a broadened p peak, but a small LDOS minimum appears. A randomly created double bond may be found in

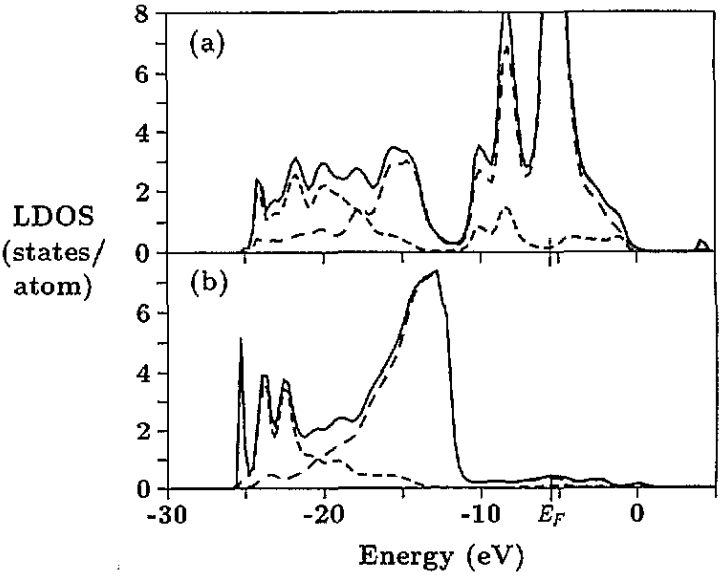

Figure 6. Local densities of states of a twofold-coordinated (*a*), and a fourfold-coordinated atom (*b*) (full curves). Short-dash curves: s partial LDOS; long-dash curves: p partial LDOS.

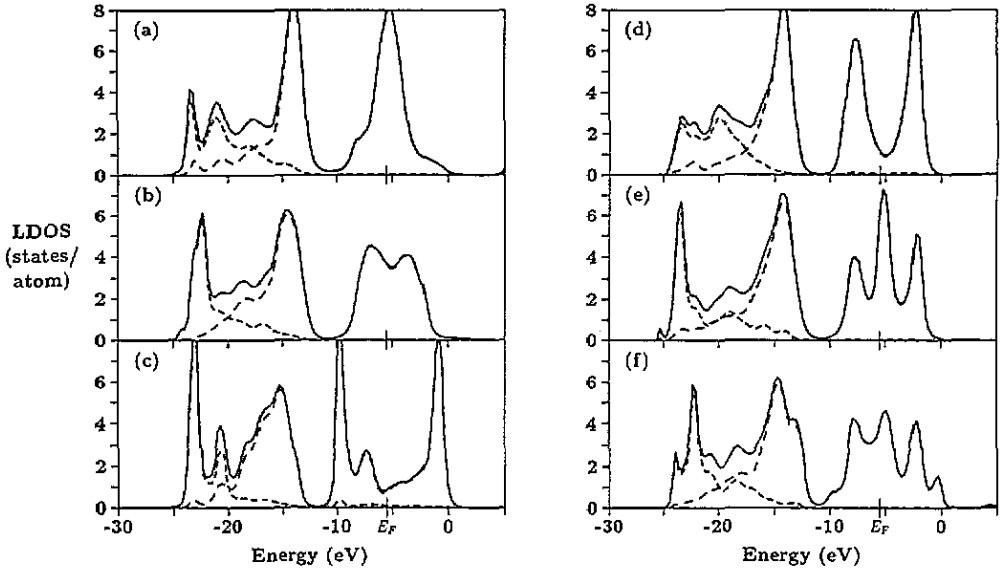

Figure 7. Local densities of states of threefold-coordinated atoms (full curves); see the text for a detailed explanation. The meaning of the broken curves is as in figure 6.

figure 7(*c*), where the bonding and antibonding π states may be clearly seen. Additionally, in this figure there are small contributions from other atoms.

As stated above, the investigated structures also contain some π bonded atom groups which give rise to further bonding and non-bonding states. Figures 7(*d*) and (*e*) show the

LDOS at atoms in the centre and at an end of a three-atom cluster, respectively. The creation and location of the bonding and non-bonding states is again straightforward from simple Hückel theory. The last example in figure 7 eventually describes an atom that belongs to a larger cluster with more (seven) atoms. The relatively high number of interactions results in the complicated structure of the defect LDOS of this atom.

To discuss briefly the case of fourfold-coordinated atoms, we note the small number of these atoms even in the high-density structure. These atoms, primarily surrounded by an under-coordinated environment, are well relaxed by the Tersoff potential. This can be seen by the small standard deviations ($\leqslant 11°$) of the bond angles in table 1. The formally complete chemical bond saturation, therefore, produces a distinct minimum LDOS region around E_F, which is determined by deviations from the diamond short-range order superimposed with small contributions from neighbouring atoms (figure 6(*b*)). These results agree well with calculations on continuous random network models for a-C in which all atoms are fourfold coordinated [26]. The DOS of these models exhibit a band gap at E_F that turns into a region of low density of states for increasing off-diagonal disorder.

4. Conclusions

In this paper, we have investigated the structural and electronic properties of a-C models with different densities, which were relaxed by means of the empirical Tersoff potential in an NVE ensemble. The calculated radial distribution functions of the generated networks qualitatively exhibit the same features as experimental curves. The mean bond lengths and bond angles have the expected values. These general facts could be satisfactory, but there are some difficulties which imply that a characterization of the computer-generated networks under only the aspect of the quantities noted above is insufficient.

All structures show a strong predominance of sp^2-bonded atoms. This fact seems to agree with the conception of Angus that hydrogen atoms are needed to permit greater fractions of sp^3 carbon atoms [2]. Actually, the lower-density systems may be related to the sp^2-rich soft a-C films [7, 8]. For the high-density model, however, this abundance of sp^2 atoms contradicts recent experimental findings [3–6]. We believe this is due to the handling of sp^2 atoms as graphitic ones by the Tersoff potential. This means that all sp^2 atoms 'feel' a delocalized π electron cloud giving rise to the graphite-like energy gain of mesomery. These atoms, therefore, are *a priori* comparable in energy (or even slightly preferred) to sp^3 atoms. Such a treatment, however, cannot be correct for amorphous systems. Additionally, a π-like interaction term that must depend on the dihedral angles between free orbitals is missing in the potential used. As a consequence, π bonds or π-bonded clusters are only created at random, leading to the emergence of distinct defect bands near E_F. We have shown how these bands arise from the unsaturated and uncorrelated atomic orbitals. The weight of these bands decreases unambiguously with a decreasing number of such defects, i.e. with increasing mass density. The large number of non-bonding π states, however, created first from effectively unbonded p orbitals, remains nearly equal for all structures. These states are mainly responsible for the TDOS maximum at E_F.

Owing to the large number of defects, all of our Tersoff-relaxed structures must be considered as electronically unstable. These problems can only be tackled by a proper treatment of under-coordinated atoms which is a sophisticated task within an empirical-potential framework. There have been a few attempts in this direction, but the analytical expressions of these potentials contain a large number of parameters, and the computational effort seems to be high. First applications, therefore, are still limited to crystalline carbon structures including defects [13].

We believe that further progress in generating and optimizing empirical potential concepts is necessary, because the use of these potentials has been advantageous for the theoretical relaxation of very large systems, which cannot be handled by *ab initio* methods.

Acknowledgments

The authors wish to thank Dr Th Frauenheim and Mr G Jungnickel for many valuable discussions. This work received support from the Deutsche Forschungsgemeinschaft under contract number Fr 889/1–1.

References

[1] Angus J C and Hayman C C 1988 *Science* **241** 913
[2] Angus J C 1991 *Diamond Relat. Mater.* **1** 61
[3] McKenzie D R, Muller D, Pailthorpe B A, Wang Z H, Kravtchinskaia E, Segal D, Lukins P B, Swift P D, Martin P J, Amaratunga G, Gaskell P H and Saeed A 1991 *Diamond Relat. Mater.* **1** 51
[4] McKenzie D R, Muller D and Pailthorpe B A 1991 *Phys. Rev. Lett.* **67** 773
[5] Gaskell P H, Saeed A, Chieux P and McKenzie D R 1991 *Phys. Rev. Lett.* **67** 1286
[6] Rother B, Siegel J, Breuer K, Mühling I, Deutschmann S, Vetter J, Trommer G, Rau B and Heiser C 1991 *J. Mater. Res.* **6** 101
[7] Li F and Lannin J S 1990 *Phys. Rev. Lett.* **65** 1905
[8] Pan H, Pruski M, Gerstein B C, Li F and Lannin J S 1991 *Phys. Rev.* B **44** 6741
[9] Demichelis F, Pirri C F and Tagliaferro A 1992 *Phys. Rev.* B **45** 14364
[10] Tersoff J 1988 *Phys. Rev. Lett.* **61** 2879
[11] Cook S J, Clancy P 1993 *Phys. Rev.* B **47** 7686
[12] Brenner D W 1990 *Phys. Rev.* B **42** 9458
[13] Heggie M I 1991 *J. Phys.: Condens. Matter* **3** 3065
[14] Kelires P C 1993 *Phys. Rev.* B **47** 1829
[15] Jungnickel G 1993 *PhD thesis* TU Chemnitz-Zwickau
[16] Frauenheim T, Blaudeck P, Stephan U and Jungnickel G 1993 *Phys. Rev.* B **48** 4823
[17] Heine V, Bullett D W, Haydock R and Kelly M J 1980 *Solid State Physics* **35** (New York: Academic)
[18] Nex C M M 1978 *J. Phys. A: Math. Gen.* **11** 653
[19] Monkhorst H J and Pack J D 1976 *Phys. Rev.* B **13** 5188
[20] Anlage S M and Smith D L 1986 *Phys. Rev.* B **34** 2336
[21] Krajči M 1987 *J. Phys. F: Met. Phys.* **17** 2217
[22] Jensen P, Meaudre R and Meaudre M 1990 *J. Phys.: Condens. Matter* **2** 4785
[23] Blaudeck P, Frauenheim T, Jungnickel G and Stephan U 1993 *Solid State Commun.* **85** 997
[24] Stephan U and Blaudeck P 1993 unpublished
[25] Blaudeck P, Frauenheim Th, Porezag D, Seifert G and Fromm E 1992 *J. Phys.: Condens. Matter* **4** 6389
[26] Koslowski T and von Niessen W 1992 *J. Phys.: Condens. Matter* **4** 6109